A three-parameter model for predicting acoustic velocities in transversely isotropic rocks under arbitrary stress

Romain Prioul and Andrey Bakulin, Schlumberger Cambridge Research; Victor Bakulin, Houston, Consultant*

Summary

Estimating subsurface stress or pore pressure from seismic velocities typically relies on specific petrophysical relationships. Most of the commonly used velocity-stress equations are designed for isotropic media and describe single (P- or S-wave) velocity versus confining stress or depth. Applying such relationships to anisotropic formations under non-hydrostatic stress state produces significant errors, especially if the relationships were calibrated from log data along deviated wells. Here, we discuss a different way of modeling and calibration of stress-dependent velocities which uniformly applies to both P- and S-wave velocities and accounts for anisotropy and a non-hydrostatic stress state.

We use non-linear elasticity theory which provides straightforward relationships between the full tensor of "effective" elastic stiffnesses and an arbitrary stress state. To describe stress-dependent velocities in isotropic material, two unstressed moduli and three non-linear elastic constants are needed. More realistic model for reservoir rock is represented by transversely isotropic media with a vertical symmetry axis (VTI) which requires five unstressed elastic moduli. Analysis of available experimental data on VTI samples suggests that stress-dependent stiffness tensor and any derived velocity are well-described by the same three "isotropic" non-linear constants, thus greatly simplifying the modeling.

We apply our technique to two different VTI samples: Jurassic North Sea shale and Colton sandstone and demonstrate good applicability of a simple three-parameter model. As non-linear coefficients can be derived directly from modern multi-mode acoustic measurements in the wells, the proposed model represents a powerful tool for predicting stress-dependent anisotropic velocities and for their inversion to stress and pore pressure.

Introduction

The relationship between seismic velocities and effective stress is a critically important element in the seismic characterization and monitoring of the subsurface stress field, either in the overburden or in the reservoir. The growing popularity of multicomponent data means that the S-velocity field may be jointly used with the P-velocity to accomplish these tasks. Utilizing multicomponent data requires a unified model which links all velocities to stress and accounts for seismic anisotropy. Here we propose a simple three-parameter model which gives such a concise and unified description to anisotropic P and S velocities under arbitrary stress. The model accounts for VTI anisotropy of unstressed rocks which can be present in most sedimentary basins. The parameters of this model can be estimated from either lab measurements or directly from borehole multi-mode acoustics (Sinha, 1996, 2001).

Theory

The Hooke's law for VTI unstressed rock is given by

$$\begin{pmatrix} T_{11} \\ T_{22} \\ T_{33} \\ T_{23} \\ T_{13} \\ T_{12} \end{pmatrix} = \begin{pmatrix} c^0_{11} & c^0_{12} & c^0_{13} & 0 & 0 & 0 \\ c^0_{12} & c^0_{11} & c^0_{13} & 0 & 0 & 0 \\ c^0_{13} & c^0_{13} & c^0_{33} & 0 & 0 & 0 \\ 0 & 0 & 0 & c^0_{44} & 0 & 0 \\ 0 & 0 & 0 & 0 & c^0_{44} & 0 \\ 0 & 0 & 0 & 0 & 0 & c^0_{66} \end{pmatrix} \begin{pmatrix} E_{11} \\ E_{22} \\ E_{33} \\ E_{23} \\ E_{13} \\ E_{12} \end{pmatrix}, \quad (1)$$

where T_{ij} and E_{ij} are corresponding stresses and strains, c^0_{ij} represents unstressed (or reference state) stiffnesses with $c^0_{12} = c^0_{11} - 2c^0_{66}$. "Effective elastic stiffnesses" c_{ij}, defining acoustic velocities under stress, can be obtained by considering the propagation of small amplitude waves in the presence of initial stresses in the medium (Sinha and Kostek, 1996; Bakulin et al., 2000). If one of the principal stresses is vertical, then $T_{23} = T_{13} = T_{12} = E_{23} = E_{13} = E_{12} = 0$ and equations take a particularly simple form:

$$\begin{aligned}
c_{11} &= c^0_{11}(1 + 2E_{11}) + T_{11} + c_{111}E_{11} + c_{112}(E_{22} + E_{33}), \\
c_{22} &= c^0_{11}(1 + 2E_{22}) + T_{22} + c_{111}E_{22} + c_{112}(E_{11} + E_{33}), \\
c_{33} &= c^0_{33}(1 + 2E_{33}) + T_{33} + c_{111}E_{33} + c_{112}(E_{11} + E_{22}), \\
c_{12} &\simeq c^0_{12}(1 + E_{11} + E_{22}) + c_{112}(E_{11} + E_{22}) + c_{123}E_{33}, \\
c_{13} &\simeq c^0_{13}(1 + E_{11} + E_{33}) + c_{112}(E_{11} + E_{33}) + c_{123}E_{22}, \\
c_{23} &\simeq c^0_{13}(1 + E_{22} + E_{33}) + c_{112}(E_{22} + E_{33}) + c_{123}E_{11}, \\
c_{66} &\simeq c^0_{66}(1 + 2E_{22}) + T_{11} + c_{144}E_{33} + c_{155}(E_{11} + E_{22}), \\
c_{55} &\simeq c^0_{44}(1 + 2E_{33}) + T_{11} + c_{144}E_{22} + c_{155}(E_{11} + E_{33}), \\
c_{44} &\simeq c^0_{44}(1 + 2E_{33}) + T_{22} + c_{144}E_{11} + c_{155}(E_{22} + E_{33}),
\end{aligned} \quad (2)$$

where c_{111}, c_{112} and c_{123} are third-order (nonlinear) elastic constants describing stress-sensitivity and $c_{144} = (c_{112} - c_{123})/2$ and $c_{155} = (c_{111} - c_{112})/4$. We adopt the convention that compressive stress is with a negative sign while tensile is positive (Sinha and Kostek, 1996).
Key assumption in equations (2) is that although the second-order elastic tensor is described by VTI media, the third-order elastic tensor is approximated by an isotropic form requiring only three third-order constants. Such a description was previously utilized for construction materials (Guz et al., 1977) and rocks (Bakulin and Protosenya, 1982; Bakulin et al., 2000), however they all used an "isotropic" approximation to convert strain into

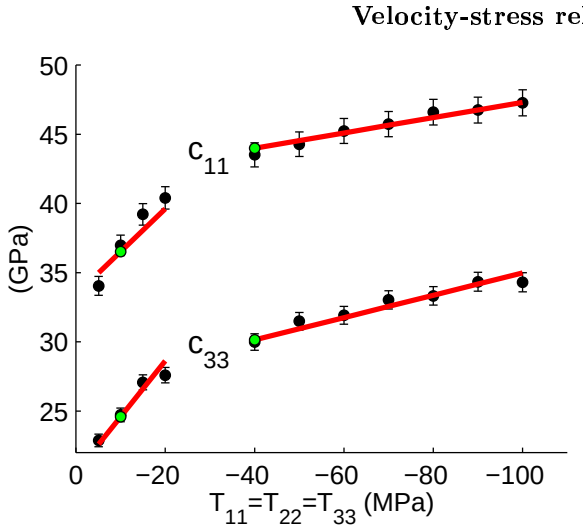

Fig. 1: Effective elastic stiffnesses c_{11} and c_{33} in two intervals of effective pressure (5-20 and 40-100 MPa) for North Sea shale (Hornby, 1995). Measured data are points and predicted data by equations (2) are lines. For 5-20 MPa, the reference state (grey/green point) was taken at 10 MPa (Thomsen parameters $V_{P0} = 3.11\ km/s$, $V_{S0} = 1.53\ km/s$, $\epsilon = 0.24$, $\delta = 0.13$, $\gamma = 0.41$). For 40-100 MPa, it was taken at 40 MPa ($V_{P0} = 3.44\ km/s$, $V_{S0} = 1.77\ km/s$, $\epsilon = 0.23$, $\delta = 0.11$, $\gamma = 0.36$.)

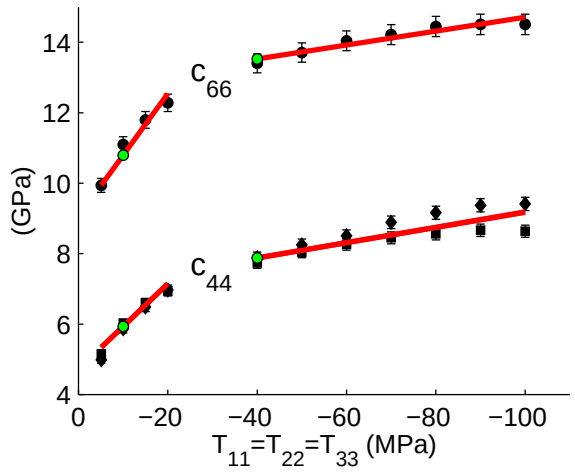

Fig. 2: Effective elastic stiffnesses $c_{66} = \rho V_{12}^2$ (●), $c_{44} = \rho V_{13}^2$ (■) and $c_{44} = \rho V_{31}^2$ (◆) in two intervals of effective pressure 5-20 and 40-100 MPa for North Sea shale. Measured data are points and predicted data by equations (2) are lines. The reference states for each stress interval are grey/green points (10 and 40 MPa).

stress in equations (2). In contrast, we propose to employ VTI Hooke's law (1) exactly. This makes it possible to use confining stress experiments for estimating all three non-linear constants. In fact, even for confining stress ($T_{11} = T_{22} = T_{33}$), VTI Hooke's law (1) predicts that $E_{11} = E_{22} \neq E_{33}$ which leaves five linearly independent equations in (2). If the amount of anisotropy is sufficient then any three out of the five (independent) equations (2) can be inverted for three non-linear coefficients c_{111}, c_{112} and c_{123}. Two remaining equations (stiffnesses) can then be predicted and compared with the measured ones to verify the validity of the original assumption on the three independent parameters. In contrast, the isotropic Hooke's law ($c_{11}^0 = c_{33}^0$, $c_{44}^0 = c_{66}^0$, $c_{13}^0 = c_{12}^0$) predicts for confining stress that $E_{11} = E_{22} = E_{33}$ which leaves only two linearly independent equations in formulas (2). From these two equations one can only estimate two combinations of three unknown non-linear coefficients, c_{111}, c_{112} and c_{123}. To determine all three of them, a non-hydrostatic stress state is required.

Clearly, in the general case of triaxial stress ($T_{11} \neq T_{22} \neq T_{33}$), equations (2) describe an orthorhombic medium in which stiffnesses are linearly dependent on principal stresses.

Jurassic North Sea shale

As our first example, we take data from compressional and shear wave velocities measured on a shale sample (Hornby, 1995) under control of both confining (P_c) and pore (P_p) pressure (P_c between 5 and 110 MPa, P_p=0 or 20 MPa). The samples of Jurassic age were drag samples from North Sea (ρ=2540 kg/m^3). This shale exhibits transversely isotropic behavior with a symmetry axis (x_3) orthogonal to fine bedding planes. This set of measurements includes velocities V_{ij} propagating along the x_i-axis with a polarization along the x_j-axis (V_{33}, V_{31}, V_{32}, V_{11}, V_{13}, V_{12}) and velocities propagating at an angle (45°) to the symmetry axis (V_{qP45}, V_{qSV45}, V_{qSH45}). All the measurements have been interpreted as phase velocities with an estimated error of ±0.5% and inverted for second-order VTI elastic constants c_{ij}^0 for each confining pressure (Figures 1, 2 and 3). As the data clearly exhibits a distinctly different behavior at low and high effective stresses (defined here as the difference between confining and pore pressures), we have divided the stress range into two intervals, 5-20 and 40-100 MPa. For each interval, along-axes quantities ($c_{11} = \rho V_{11}^2$, $c_{33} = \rho V_{33}^2$, $c_{66} = \rho V_{12}^2$, and $c_{44} = \rho V_{13}^2 = \rho V_{31}^2 = \rho V_{32}^2$) have been inverted for three third-order constants c_{111}, c_{112}, c_{123} (Table 1) by minimizing the least-squares misfit function (χ^2) between measured stiffnesses and those predicted by equations (2). Figures 1 and 2 prove that three "isotropic" third-order coefficients provide a good description for four VTI stiffnesses in each stress interval. The error bounds on the derived non-linear constants (Table 1) were estimated using quantitative confidence limits derived from a Monte-Carlo simulation and using the χ^2 function as a statistical measure of goodness-of-fit.

Table 1: Third-order elastic constants obtained from confining stress experiment on a North Sea shale (Hornby, 1995).

Confining (MPa)	$c_{111} \pm \Delta c_{111}$ (GPa)	$c_{112} \pm \Delta c_{112}$ (GPa)	$c_{123} \pm \Delta c_{123}$ (GPa)
5-20	-11300±2900	-4800±2500	5800±4000
40-100	-3100±600	-800±500	40±800

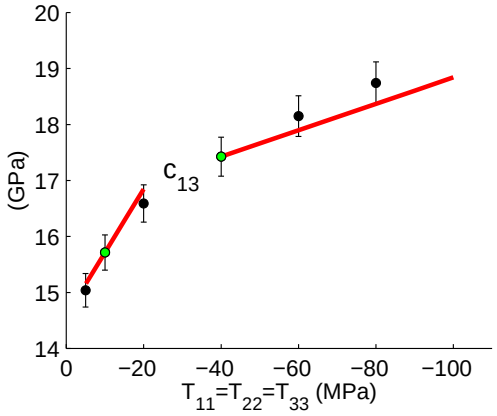

Fig. 3: Measured (points) and predicted (lines) effective elastic stiffness c_{13} in two intervals of effective pressure (5-20 and 40-100 MPa) for North Sea shale (Hornby, 1995). The prediction is done with equations (2) where parameters c_{111}, c_{112}, c_{123} were inverted from c_{11}, c_{33}, c_{44} and c_{66}.

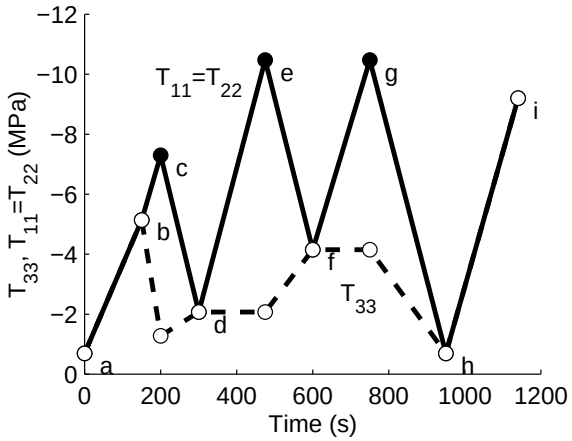

Fig. 4: Loading cycle of the triaxial pressure cell with Colton sandstone (Dillen et al., 1999). Principal stresses T_{11} and T_{22} were maintained equally to preserve the transverse isotropy of the sample.

The standard deviations on the measured stiffnesses have been estimated to be ± 2 %. As an independent check of our model, we can predict the remaining stiffness c_{13}^{pred} which was not involved in the inversion for non-linear constants and compare it with c_{13}^{meas} estimated from off-axes velocities V_{qP45} and V_{qSV45}. Such a comparison is plotted on Figure 3 and confirms a good *a posteriori* prediction.

Colton sandstone

As our second example, we take ultrasonic measurements on a dry Colton sandstone placed in a triaxial pressure machine (Dillen et al., 1999). The Colton sandstone formation is an Eocene fluvial deposit located in north-central Utah in the United States (ρ=2380 kg/m^3, porosity $\phi = 13\%$).

At zero stress, the Colton sandstone also exhibits transversely isotropic behavior with the symmetry axis aligned with one of the directions of the triaxial machine (T_{33}). Equal compressive stresses were applied in the directions x_1 and x_2 to preserve the VTI anisotropy of the sample ($T_{11} = T_{22}$). The block was subjected to a load cycle, $a-b-c-d-e-f-g-h-i$, as a function of time (Figure 4). The stress path contains both hydrostatic or confining ($T_{11} = T_{22} = T_{33}$) intervals (e.g. $h-i$) as well as non-hydrostatic ones (e.g. $b-h$), so we can compare the non-linear coefficients retrieved at different stress states and estimate the stability of the inversion.

The complete data set includes only velocities of compressional and shear wave propagating along the coordinate axes. This allows us to compute four VTI stiffnesses: $c_{11} = \rho V_{11}^2 = \rho V_{22}^2$, $c_{33} = \rho V_{33}^2$, $c_{66} = \rho V_{21}^2 = \rho V_{12}^2$, and $c_{44} = \rho V_{13}^2 = \rho V_{23}^2 = \rho V_{32}^2 = \rho V_{31}^2$. Measured velocities defining the same stiffness (Figure 5 and 6) are approximatively equal ($V_{11} \sim V_{22}$, $V_{21} \sim V_{12}$ and $V_{13} \sim V_{23} \sim V_{32} \sim V_{31}$), so we have used all of them simultaneously in the least-squares inversion.

Third-order elastic constants for Colton sandstone were estimated following the same procedure as for the shale. The reference state was taken at zero time ($T_{11} = T_{22} = T_{33}$=-0.7 MPa) and Thomsen parameters were estimated as $V_{P0} = 2.77\ km/s$, $V_{S0} = 1.89\ km/s$, $\epsilon = 0.05$, $\gamma = 0.03$. Thomsen parameter δ was not constrained by the measured velocities along axes and was taken as 0.05 in this study. Estimation of the non-linear coefficients at confining ($h-i$) and arbitrary ($a-i$) stress states led to the same coefficients although confidence limits in the latter were approximately three times smaller (Table 2). Increased uncertainty for the confining stress is easily understood from equations (2) when these are viewed as a set of linear equations with respect to unknowns c_{111}, c_{112} and c_{123}. If an isotropic sample is subjected to confining stress then it stays isotropic and the matrix of coefficients in (2) is singular, because $E_{11} = E_{22} = E_{33}$. With only two equations being linearly independent, one can constrain only two combinations out of three non-linear constants. Intrinsic anisotropy and/or non-hydrostatic stress makes E_{11}, E_{22}, E_{33} different and removes the singularity.

Table 2: Third-order elastic constants for Colton sandstone under confining and arbitrary stress between 0-11 MPa.

Stress (MPa)	$c_{111} \pm \Delta c_{111}$ (GPa)	$c_{112} \pm \Delta c_{112}$ (GPa)	$c_{123} \pm \Delta c_{123}$ (GPa)
$(h-i)_{\text{confining}}$	-7100±2000	-1300±1200	700±2000
$(a-i)_{\text{arbitrary}}$	-7400±800	-1400±500	600±800

However, due to the weak anisotropy of the Colton sandstone, confining stress makes $E_{11}(= E_{22})$ and E_{33} only slightly different. Therefore the condition number of the matrix of coefficients from (2) is still high because coefficients are close to those of a singular case of isotropy. In contrast, the deviatoric stress state ($T_{11} = T_{22} \neq T_{33}$) moves $E_{11}(= E_{22})$ and E_{33} further apart, thus decreas-

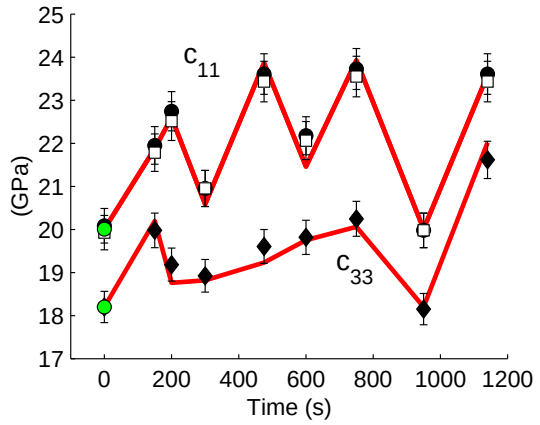

Fig. 5: Measured (points) and predicted (lines) effective elastic stiffnesses $c_{11} = \rho V_{11}^2$ (●), $c_{11} = \rho V_{22}^2$ (□) and $c_{33} = \rho V_{33}^2$ (◆) for the Colton sandstone. Error bars on measured stiffnesses correspond to ±2 %. Only three parameters, c_{111}, c_{112}, c_{123}, have been used to predict all stiffnesses under the entire loading cycle. The reference state (grey/green points) has been taken at zero time ($T_{11} = T_{22} = T_{33} = -0.7\ MPa$).

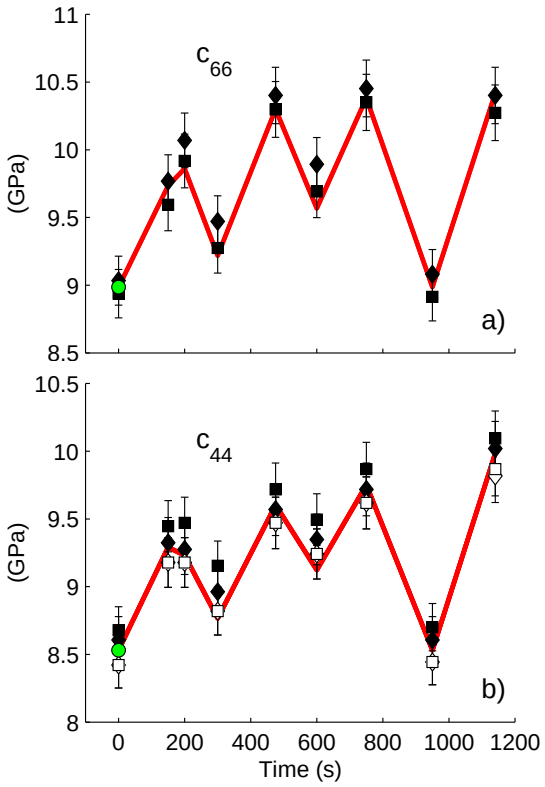

Fig. 6: Measured and predicted effective elastic stiffnesses for Colton sandstone: (a) $c_{66} = \rho V_{12}^2$ (◆) and $c_{66} = \rho V_{21}^2$ (■); (b) $c_{44} = \rho V_{23}^2$ (◇), $c_{44} = \rho V_{32}^2$ (□), $c_{44} = \rho V_{13}^2$ (◆), $c_{44} = \rho V_{31}^2$ (■). Error bars on measured stiffnesses correspond to ±2 %. Only three parameters, c_{111}, c_{112}, c_{123}, have been used to predict all stiffnesses under the entire loading cycle. The reference state (grey/green point) for stiffnesses c_{66}^0 and c_{44}^0 has been taken at zero time ($T_{11} = T_{22} = T_{33} = -0.7$ MPa).

ing the condition number of the matrix of coefficients and decreasing the confidence limits in the solution. Figures 5 and 6 demonstrate that overall measured stiffnesses are well described by a solid curve representing the predictions based on equations (2) and third-order elastic constants derived from the second row of Table 2.

Discussion and conclusions

We have proposed a concise and comprehensive way of velocity-stress modeling based on simplified non-linear elasticity theory. The advantages of the suggested modeling scheme are:

- Both P and S ($S1$ and $S2$) velocities are treated using the same physical framework. As a result *any velocity* in *any direction* can be predicted as a function of stress.
- Intrinsic anisotropy of unstressed formations is automatically included.
- The model allows an arbitrary triaxial stress state ($T_{11} \neq T_{22} \neq T_{33}$) and therefore predicts any velocity for general non-hydrostatic stress.
- Only three (stress-independent) constants are required to describe stress variation of any velocity.
- Well calibration of the model may be performed directly in-situ using multi-mode borehole acoustic measurements (Sinha, 1996, 2001).

The minor disadvantage of the model is that it operates within a limited stress interval; this may not be a problem if a window of anticipated effective stress is not too large for selected depth interval.

References

Bakulin, V. N. and Protosenya, A. G., 1982, Nonlinear effects in travel of elastic waves through rocks: Proc. USSR Acad. Sc. (Dokl.Akad.Nauk SSSR), **263** (2), 314–316.

Bakulin, A. V., Troyan, V. N., and Bakulin, V. N., 2000, Acoustoelasticity of rocks St. Petersburg Univ. Press (in Russian).

Dillen, M. W. P., Cruts, H. M. A., Groenenboom, J., Fokkema, J. T., and Duijndam, A. J. W., 1999, Ultrasonic velocity and shear-wave splitting behavior of a Colton sandstone under a changing triaxial stress: Geophysics, **64**, no. 5, 1603–1607.

Guz, A. N., Makhort, F. G., and Guscha, O. I., 1977, Introduction to acoustoelasticity, Kiev, "Naukova dumka" (in Russian).

Hornby, B. E., 1995, The elastic properties of shales: Ph.D. dissertation, University of Cambridge, UK.

Sinha, B. K., and Kostek, S., 1996, Stress-induced azimuthal anisotropy in borehole flexural waves: Geophysics, **61**, 1899–1907.

Sinha, B. K., 1996, Estimation of formation nonlinear constants by sonic measurements while changing borehole pressures: 66th Annual Internat. Mtg., Soc. Expl. Geophys., Expanded Abstracts, 118–121.

Sinha, B. K., 2001, Stress-induced changes in the borehole stoneley and flexural dispersions: 71th Annual Internat. Mtg., Soc. Expl. Geophys., Expanded Abstracts, this volume.